Poster2-108 **DUAL-RADAR OBSERVASTION STUDY OF SQUALL LINES IN CHINA**

HaiGuang Zhou *
Chinese Academy of Meteorological Science, Beijing, P. R. China

1. INTRODUCTION

The squall line is a linear mesoscale convective system, which can produce gale, heavy precipitation, hail, and other severe weathers (Zipser, 1977; Braun and Houze, 1994; Xue, 2002; Sun and Wang, 2013; Kalina et al, 2014; Wakimoto et al, 2015; Cazenave et al, 2016; Stechman et al, 2016; Alfaro, 2017; Rosenow et al, 2018). Doppler radar is a powerful tool to investigate the 3D kinematic structure of the convective system (Braun and Houze, 1994; Jeong et al, 2012; Wakimoto et al, 2015; Cazenave et al, 2016). Dual-Doppler radar retrieval wind fields play an important role on studying the squall line kinematic structure (Smull and Houze,1987; Chong and Bousquet, 1999; Jung et al, 2012; Chang et al 2015; Zhou, 2016; Conrad and Knupp, 2019). China New Generation Doppler Weather Radar (CINRAD) has been operated for more than 20 years. There are more than 200 Doppler weather radars in the mainland. This study focused on the 3D kinematic structure of the squall lines with the dual-Doppler radar retrieval data. Three squall lines were investigated. The first case is on 31 March 2014 in the South China (hereafter referred to as SC), the second case is on 14 June 2009 in the Yangtse-Huaihe River (hereafter referred to as YH), and the last one is on 16 September 2008 in the North China (hereafter referred to as NC). The structure differences of these cases were also discussed.

2. DATA AND METHODOLOGY

Three Dual-Doppler networks were employed to retrieve the 3D wind fields. Guangzhou-Shenzhen dual-Doppler was employed to retrieve the wind fields of SC case (Fig. 1a), Nanjing-Maanshan dual-Doppler for YH case (Fig. 1b), and Beijing dual-Doppler for SC case (Fig. 1c). The radar data was processed by the quality control algorithm. Then, the wind fields were retrieved by the multiple-Doppler synthesis and continuity adjustment technique (MUSCAT) (Bousquet and Chong, 1998, Bousquet and Tabary, 2014). We applied this algorithm to the ground-based dual-Doppler wind retrieve, and studied the kinematic structure of the squall line (Zhou, 2016) and the supercell thunderstorm (Zhou, 2018). The other data included the automatic weather station data, and the sounding data.

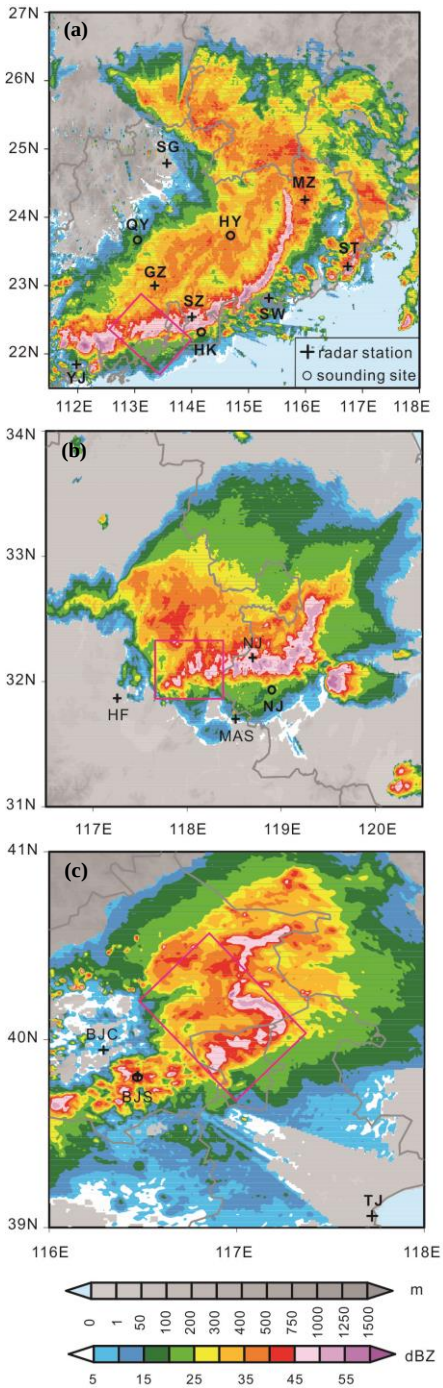

Fig.1. Map of the dual-Doppler radar observation network. The color shading shows the composite reflectivity (dBZ), the gray shading for the altitude (m), and the rectangles for the dual-Doppler wind retrieval domain. (a) shows Guangzhou-Shenzhen dual-Doppler and the composite reflectivity at 0900 LST 31 March 2014, (b) for Nanjing-Maanshan dual-Doppler and the composite reflectivity at

* *Corresponding author address:* HaiGuang Zhou, Chinese Academy of Meteorological Science, Beijing 100081, P. R. China; e-mail: zhouhg@cma.gov.cn

1830 LST 14 June 2009, and (c) for Beijing dual-Doppler and the composite reflectivity at 1848 LST 16 September 2008.

3. RESULTS

3.1 *Kinematic Structure of SC Squall Line*

On 2000 LST 30 March 2014, the warm and moist flow from China South Sea prevailed at the low layer of the south China. On the other hand, the cold and dry air prevailed at the middle and the upper layer. The vertical shear was about 30 m/s between 0- and 6 km altitude at 0800 LST 31 March. A squall line developed in Guangxi province. It passed through Guangdong province, which caused gale, heavy rainfall, and hail.

Fig. 2 presents the radar reflectivity and the storm-relative wind filed at 0918 LST 31 March 2014. At the lower altitudes, the reflectivity gradient was intense at the leading edge. The intense reflectivity band more than 50 dBZ was observed in the squall front. The leading edge was oriented in the southwest-northeast direction (Fig. 2a). The storm-relative front-to-rear inflow was strong along the leading edge. The maximum inflow was about 20 m/s. As shown in Fig. 2a, a new convective cell was developing at the front of the leading edge. The front-to-rear inflow and the rear-to-front cold inflow converged at the convective line. It resulted in the updraft (Fig. 2c) and the convergence band (Fig. 2d). The maximum updraft was more than 9 m/s. Some convergence centers were observed in the convergence band (Fig. 2d). The absolute value of the strongest convergence was more than 55×10^{-4} /s. At 5 km altitude, the storm-relative front-to-rear horizontal inflow prevailed (Fig. 2b).

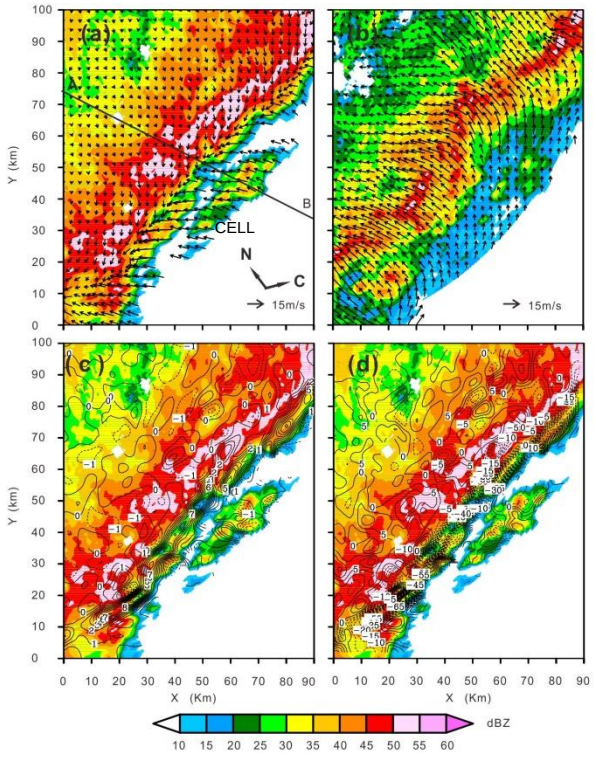

Fig. 2. The storm-relative horizontal wind fields at 1.5 km (a) and 5 km (b) at 0918 LST 31 March 2014. (c) for the vertical velocity, and (d) for the divergence field velocities at 1.5 km. The solid lines indicate the updraft, and the dashed lines for the downdraft (c). Solid lines are for positive values (divergence), and dashed lines for the negative value (convergence); the contour interval is 5×10^{-4} s^{-1}. The *x* axis and *y* axis are, respectively, parallel and perpendicular to the dual-radar baseline. The squall line movement direction (*C*), and the north (*N*) are indicated in (a). The color shading is radar reflectivity (dBZ).

As indicated in Fig. 3, the storm-relative front-to-rear horizontal flow entered the squall line from the surface to the altitude of 6 km at the leading edge, which was associated with the intense upward motion. Above 6 km height, part of the storm-relative front-to-rear flow slopped forward and outward, and the other part of the flow rearward. The maximum inflow was more than 20 m/s at the 5-8 km altitude in the convective region. The forward flow formed the overhanging echo at the middle and upper altitudes of the leading edge. The rearward flow prevailed in the stratiform region above 4 km altitude. The updrafts in the convective region were about 13 m/s at the height of 6 km. On the other hand, the storm-relative rear-to-font horizontal dry cold inflow entered the stratiform region below 4 km height. The inflow attained the maximum value of more than 6 m/s at the altitude of 2 km. This inflow played an important role in feeding the dry and cold air. Three flows were presented in this squall line. The first flow was the storm-relative front-to-rear inflow at the low layer of the convective cloud region. The second flow was the outward flow at the middle and upper layer of the convective region. The third flow was the storm-relative rear-to-front inflow below 4 km altitude at the stratiform cloud region. On the other hand, the storm-relative rear-to-front inflow entered the stratiform region blow 3 km height in the previous squall line in the same area (Zhou, 2016). A new convective cell was observed at the front of the squall line (*r* =65~80km), due to the moist air convergence by the storm-relative front-to-rear inflow at the lower altitudes.

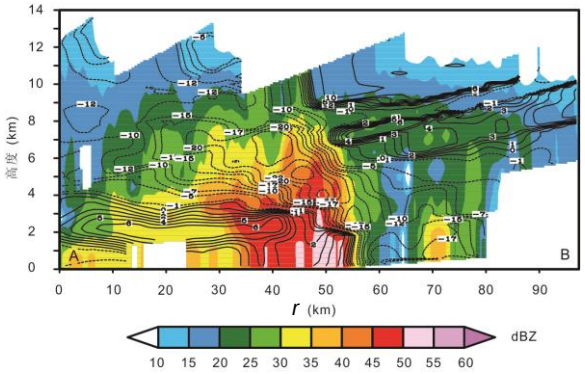

Fig. 3. Reflectivity, and the storm-relative horizontal flow in the vertical cross-section perpendicular to the squall line (along AB in Fig. 2a).

3.2 *Kinematic Structure of YH Squall Line*

On 0800 LST 14 June 2009, a surface convergence line was located in the west of Jiangsu province. This was conducive to the moist convergence. A weak shear line was observed at the low level. The value of the convective available potential energy (CAPE) was approximately 1200 J/kg in the center area of Jiangsu.

This large CAPE denoted that the presquall environment was convectively unstable, and was favourable for the squall line development. On 1800 LST 14 June, the mature squall line entered into Nanjing-Mananshan dual-Doppler radar domain. The baseline was about 57.8 km length.

Fig. 4 presents the radar reflectivity and the storm-relative wind fields retrieved from the dual-Doppler. At 2 km altitude (Fig. 4a), the leading edge was oriented in the west-east direction. Some intense cells over 45 dBZ were located along the leading edge. The maximum reflectivity was more than 50 dBZ. The storm-relative front-to-rear flow transported the unstable and moist air into the convective region. The storm-relative rear-to-front flow with cold air entered the stratiform region. The convergence was prominent at the low and middle levels of the convective line. At the middle and upper level, the storm-relative front-to-rear prevailed (Fig. 4b). In the vertical cross-section (Fig. 4c), the storm-relative front-to-rear inflow entered the convective cloud region. The storm-relative rear-to-front flow prevailed below 4 km altitude in the stratiform region. The two flows converged in the convective cloud region. Above 4km altitude, the storm-relative front-to-rear flow prevailed in the convective and stratiform region. The flow structure was different from that of SC squall line.

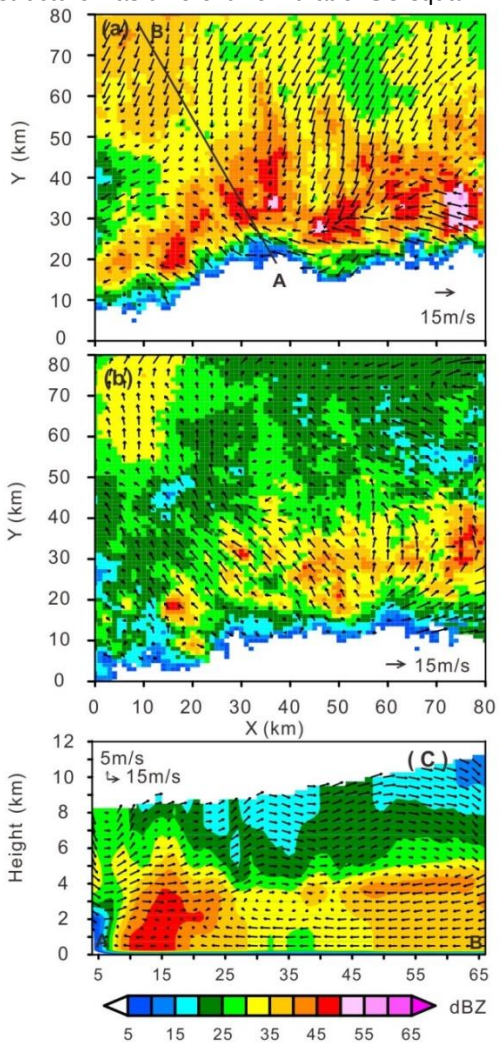

Fig. 4. The storm-relative horizontal wind fields at 2 km (a) and 5 km (b) at 1836 LST 14 June 2009. (c) for the storm-relative wind field in the vertical cross-section (along AB in a).

3.3 *Kinematic Structure of NC Squall Line*

A squall line passed through Beijing on 16 September 2008, Due to the shear line at the low and middle level, and the cold air before the trough. Fig. 5 indicated the radar reflectivity and the storm-relative wind field. At 2 km altitude (Fig. 5a), the intense convective cell was over 50 dBZ in the convective cloud region. The front-to-rear flow and the rear-to-front flow converged at the convective cloud region. The updrafts were showed in the convective region (Fig. 5c), corresponding to the convergence region and intense reflectivity. The downdrafts were observed in the stratiform region. At 5km altitude, the front-to-rear flow prevailed in the squall line (Fig. 5b). The updrafts at the middle altitude were more intense than that of the low level. In the vertical cross-section, the front-to-rear flow entered the convective region. At the altitude of 6 km, this flow changed into two flows. Part of the flow slopped forward and outward, and the other part of the flow rearward. The rear-to-front flow entered the stratiform region below the altitude of about 3km.

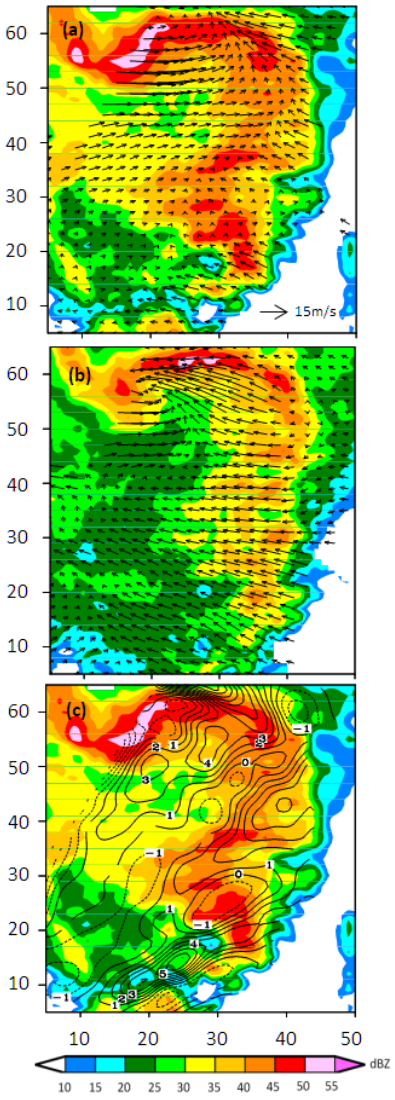

Fig. 5. The storm-relative horizontal wind fields at 2 km (a) and 5 km (b), respectively, at 1848 LST 16 September 2008. (c) denotes the vertical velocity at 2 km height. The solid lines are the updraft, and the dashed lines for the downdraft.

4. *DISCUSSIONS AND CONCLUSIONS*

Many features among the three cases were similar. The results showed that the surface convergence line played an important role on the convective band formation. The mid-altitude radial convergence (MARC) was very clear at the mid-level of the squall front, which location was corresponding to the heavy reflectivity band. The mid-altitude radial convergence was important to the formation of the convective line. It indicated that the convective cells in the squall front produced the heavy rainfall.

Moreover, the contrastive analyse was applied to the similarities and differences of the three squall line. The synoptic condition and the thermodynamic condition of the atmospheric environment played important role on the structure differences of the squall lines. The spatial scale, duration, the storm-relative wind, the convective intensity, and the local heavy rainfall in the SC squall line were the strongest in the three cases.

First, the radar echo in the SC squall line was the strongest. The horizontal and the vertical scale of the SC case was the largest, too. The horizontal scale of the NC squall line and the YH squall line were about 100 km, and 200 km respectively in the mature period. The horizontal scale of the SC squall line was more than 400 km in its mature period. Some convective bands more than 50 dBZ were located in the SC squall line convective region. In the vertical scale, the SC case was the most intensive too. The echo of 30 dBZ was about 8.5 km height in the SC squall line. On the other hand, the echo of 30 dBZ in the other two cases was 6.5 km height only.

Second, the horizontal storm-relative wind speed in SC squall line was the strongest. The convergence in the SC case was more intensive than those of the other two cases. In the SC case, the organizational characteristic of the horizontal font-to-rear flow was more remarkable than the others. In the SC squall line, the storm-relative wind speed in the convective region was up to the maximum of 20 m/s at 5-8 km altitude as showed in the vertical cross-section.

Third, the 3D wind field patterns of the three squall lines were different. The synoptic condition and the thermodynamic condition of the atmospheric environment contribute to the wind pattern. In the SC squall line, the storm-relative front-to-rear inflow entered the squall line below the altitude of 6km from the front. This inflow converted into two outward flows in the front of the convective cloud at about 5.5km height. Part of the front-to-rear inflow moved forward, and the other part sloped into the stratiform cloud. The storm-relative rear-to-font horizontal dry cold inflow entered the stratiform region below 4 km height.

In the YH squall line, the storm-relative front-to-rear inflow entered the squall line from the leading edge. The storm-relative rear-to-front inflow entered the squall line from the stratiform cloud region below the altitude of 4 km. In the convective cloud and the stratiform cloud region, the storm-relative front-to-rear flow prevailed above 4 km height.

In the NC squall line, the front-to-rear inflow directed into the squall line from the surface to the height of 5 km at the leading edge, and then converted into two outward flows. One flow was forward, and the other rearward. The rear-to-front inflow entered the NC squall line below 2 km height.

5. *REFERENCES*

Zipser, E. J., 1977: Mesoscale and convective-scale downdrafts as distinct components of squall-line structure. *Mon. Weather Rev*., 105(12), 1568-1589.

Braun, S. A. and R. A. Houze, 1994: The transition zone and secondary maximum of radar reflectivity behind a midlatitude squall line: results retrieved from Doppler radar data. *J. Atmos. Sci.*, 51(19), 2733-2755.

Xue, M., 2002: Density currents in shear flows: Effects of rigid lid and cold-pool internal circulation, and application to squall line dynamics. *Quart. J. Roy. Met. Soc.*, 128, 47-74.

Sun, J. and H. Wang, 2013: Radar data assimilation with WRF 4D-Var. Part II: Comparison with 3D-Var for a squall line over the U.S. Great Plains. *Mon. Wea. Rev.*, 141, 2245–2264, https://doi.org/10. 117 5/MWR-D-12-00169.1.

Kalina, E. A., K. Friedrich, S. M. Ellis, and D. W. Burgess, 2014: Comparison of disdrometer and X-Band mobile radar observations in convective precipitation. *Mon. Wea. Rev.*, 142, 2414–2435, https://doi.org/10.1175/MWR-D-14-00039.1.

Wakimoto, R. M., P. Stauffer, and W. C. Lee, 2015: The vertical vorticity structure within a squall line observed during BAMEX: Banded vorticity features and the evolution of a bowing segment. *Mon. Wea. Rev.*, 143, 341–362, https://doi.org/10.1175/MWR-D-14-00246.1

Cazenave, F., M. Gosset, M. Kacou, M. Alcoba, E. Fontaine, C. Duroure, and B. Dolan, 2016: Characterization of hydrometeors in Sahelian convective systems with an X-Band radar and comparison with In situ measurements. Part I: Sensitivity of polarimetric radar particle identification retrieval and case study evaluation. *J. Appl. Meteor. Climatol.*, 55, 231–249, https://doi. org/10.1175/JAMC-D-15-0013.1.

Stechman, D. M., R. M. Rauber, G. M. McFarquhar, B. F. Jewett, and D. P. Jorgensen, 2016: Interaction of an upper-tropospheric jet with a squall line originating along a cold frontal boundary. *Mon. Wea. Rev.*, 144, 4197–4219, https://doi.org/ 10.1175/MW R-D-16-0044.1.

Alfaro, D. A., 2017: Low-tropospheric shear in the structure of squall lines: Impacts on latent heating under layer-lifting ascent. *J. Atmos. Sci.*, 74, 229–248, https://doi.org/10.1175/JAS-D-16-0168.1.

Rosenow, A. A., K. Howard, and J. Meitín, 2018: Gap-filling mobile radar observations of a snow squall in the San Luis Valley. *Mon. Wea. Rev.*, 146,

2469–2481,https://doi.org/10.1175/MWR-D-17-0323.1

Jeong, J. H., D. I. Lee, C. C. Wang, S. M. Jang, C. H. You, and M. Jang, 2012: Environment and morphology of mesoscale convective systems associated with the Changma front during 9-10 July 2007. *ANN. GEOPHY.*, 30(8),1235-1248,doi:10.5194/angeo-30-1235-2012.

Smull, B. F. and R. A. Houze, 1987: Dual-Doppler radar analysis of a midlatitude squall line with a trailing region of stratiform rain. *J. Atmos. Sci.*, 44(15), 2128-2149.

Chong M. and O. Bousquet, 1999: A mesovortex within a near-equatorial mesoscale convective system during TOGA COARE. *Mon. Weather Rev.*, 127(6), 1145-1156.

Jung, S. A., D. I. Lee, J. D. Jou, and H. Uyeda, 2012: Microphysical properties of maritime squall line observed on June 2, 2008 in Taiwan. *J. of the Meteor. Soc. of Japan*, 90(5), 833-850.

Chang, W. Y., W. C. Lee, and Y. C. Liou, 2015: The kinematic and microphysical characteristics and associated precipitation efficiency of subtropical convection during SoWMEX/TiMREX. *Mon. Wea. Rev.*, 143, 317–340, https://doi.org/10.1175/MWR-D-14-0008 1.1.

Zhou, H. G., 2016: Wind structure of a subtropical squall line in China: results from dual-Doppler radar data. *Adv. in Meteor*., doi: 10.1155/2016/9059383.

Conrad, D.M. and K.R. Knupp, 2019: Doppler radar observations of horizontal shearing instability in quasi-Linear convective systems. *Mon. Wea. Rev*., 147,1297–1318, https://doi.org/10.1175/MWR-D-18- 0257.1

Bousquet, O., and M. Chong, 1998: A multiple-Doppler synthesis and continuity adjustment technique (MUSCAT) to recover wind components from Doppler radar measurements. *J. Atmos. Oceanic Technol.*, 15(2), 343-359.

Bousquet, O., and P. Tabary, 2014: Development of a nationwide real-time 3-D wind and reflectivity radar composite in France. *Quart. J. Roy. Meteor. Soc.*, 140(679), 611-625.

Zhou, H. G., 2018: Observations of 23 June 2016 EF4 tornado supercell thunderstorm mesoscale structure in Funing county, Jiangsu province. *Chinese J. Geophysics*, 61(9), 3617-3639, doi: 10.6038 /cjg2018L0166.

Acknowledgements

This research was supported by Chinese Academy of Meteorological Science under Grant CAMS-2018KJ035 and CAMS-2019KJ030.